THE EFFECT OF WELDING ON THE MICROSTRUCTURE OF THE AGE HARDENING ALUMINUM ALLOY 2219

S. D. Dumolt, D. E. Laughlin and J. C. Williams
Department of Metallurgical Engineering and Materials Science
and
The Center for the Joining of Materials
Carnegie-Mellon University
Pittsburgh, Pennsylvania 15213

INTRODUCTION

The principal feature distinguishing the heat treatable from the non-heat treatable aluminum alloys is the formation of second phase precipitates during heat treatment of the former. These precipitates generally lead to improved mechanical properties, but their structure, distribution, size, and response to outside influences will determine the degree to which these precipitates increase the usefulness of a particular alloy. The temperature variations which occur in the workpiece during welding induce marked changes in the microstructure and mechanical properties of the heat affected zone (HAZ) of heat treatable alloys.[1] These changes affect the precipitation sequence and/or cause dissolution of the strengthening precipitates and can lead to a local structure which is very different from that of the original structure.

In order to study the effect of welding on the precipitates in heat treatable alloys we chose the commercial aluminum alloy 2219. This alloy was chosen because it is weldable and because the binary alloy system on which it is based (Al-Cu) has a microstructure which has been well documented.[2,3] Further, it can be initially heat treated to contain any of the precipitates of the aluminum-rich end of the aluminum-copper binary system. If weld specimens are heat treated to contain one or more types of these precipitates prior to welding, the effect of welding-induced transient thermal conditions on the microstructure can be investigated.

The temperature cycle experienced by any point within the thermal field of a welding heat source is characterized by rapid heating followed by somewhat more gradual cooling. Because of the short times involved in the welding process, the extent to which the microstructure is affected depends to a great extent on the kinetics of the specific processes leading to microstructural alterations. In particular, the actual occurrence of potentially feasible precipitate transformations depends not only on the maximum temperature achieved, but also on the time spent in the appropriate temperature regime(s). Also, due to the fact that there is more than one type of precipitate in this alloy system, it is possible that more than one transformation may occur during the welding thermal cycle.

BACKGROUND

The age hardenable commercial aluminum alloys are classified as follows: the 2000 series (Al-Cu, Al-Cu-Mg), the 6000 series (Al-Mg-Si), and the 7000 series (Al-Zn-Mg). Although these series are based upon different alloy systems, the general features of their precipitation processes are similar and can be illustrated by the aluminum-rich end of the aluminum-copper phase diagram (Fig. 1). The alloy used in this study, 2219, contains about 6wt% copper and its aging characteristics are similar to those of an Al-Cu binary alloy. At equilibrium it contains only the aluminum-rich α and the stable Θ ($CuAl_2$) phases. During normal heat treating procedures many alloys (including all the heat treatable aluminum alloys) will form a sequence of metastable phases before the formation of the equilibrium phase. As shown in Figure 1, the Al-Cu system contains three such phases.[2,4] Upon solution treating, quenching, and aging at low temperatures ($< \sim 200°C$ (390°F)) precipitation follows the sequence characteristic of this system:[3]

$$\alpha' \rightarrow \alpha + \text{G.P. zones} \rightarrow \alpha + \Theta'' \rightarrow \alpha + \Theta',$$

where α' is the supersaturated solution of copper in aluminum resulting from the solution treatment and quench. At somewhat higher aging temperatures the $\alpha + \Theta' \rightarrow \alpha + \Theta$ reaction also occurs. Figure 2 shows transmission electron micrographs of alloy 2219 containing each of these metastable phases (GP zones, Θ'', Θ') along with their characteristic electron diffraction patterns. These are shown for easy comparison with the welding-induced microstructural changes shown later.

Gunier-Preston zones (GP zones) are the first precipitates to appear during low temperature aging. They exist as disk-shaped monolayers of copper atoms lying on the {100} planes of the aluminum matrix (the faces of the face-centered cubic aluminum unit cell). The disk diameter is less than 150Å and they are coherent with the matrix. The Θ'' phase has the same platelike shape and orientation as the GP zones but it is slightly larger in diameter ($\sim$ 200-500Å) and is intrinsically thicker. The Θ' phase has its own body-centered tetragonal structure which is different from that of the aluminum matrix. It, like G.P. zones and Θ'', exists as plates on the {100} planes, but it is much larger than either (1000-10,000Å diameter, 150Å thickness).

These precipitates exist under metastable equilibrium conditions; if a phase remains at a temperature below its solvus line, it will continue to grow and will eventually be replaced by the next phase in the sequence. The upper temperature limit for existence of each type of precipitate is its metastable solvus line (see Fig. 1). As temperatures approaching its solvus are reached, the volume fraction of the precipitate decreases until, at the solvus and above, it completely disappears. When this occurs the structure has undergone reversion.[4] The time required for this reversion to occur depends upon the size and nature of the precipitates as well as the temperature. Because of their thinness, small diameter, and coherency, it is expected that G.P. zones will revert much more quickly than a larger, thicker, semi-coherent plate like Θ''.

EXPERIMENTAL METHODS

A direct current straight polarity gas tungsten arc (GTA) autogenous weld was made on each of three 1/4" plates of alloy 2219, each initially heat treated to contain one of the three metastable precipitates of the Al-Cu system (Plates A, B, and C). The composition of the material used is given in Table I. The G.P. zones were produced in Plate A by a solution treatment in molten salt at 530°C (986°F) and a room temperature water quench (STQ) followed by an aging treatment in an air furnace at 130°C (266°F) for 12 hours. The Θ" plate (Plate B) was subjected to STQ plus an aging treatment at 160°C (320°F) for 6 hours. Θ' was produced in Plate C by STQ followed by aging at 200°C (392°F) for 24 hours. Each weld was a full penetration type in which two-dimensional heat flow in the plate is reasonably approximated which simplifies the subsequent microstructural analysis. Each of the welded plates was then systematically sectioned parallel to the welding direction starting with the initial cut at the edge of the fusion zone and successively moving into the base metal using a low speed diamond saw. The individual sections were stored in liquid nitrogen (to inhibit natural aging) until disks from them were made into thin foils for transmission electron microscopy (TEM) examination. Using TEM and electron diffraction the nature and distribution of the precipitates were characterized as a function of distance from the fusion zone.

RESULTS

Plate A - G.P. Zones[5]

The postweld macrostructure of the plate which initially contained G.P. zones is shown in Figure 3(a). Figure 3(b) is a schematic which includes the microstructural phenomena observed in the heat affected zone. The actual microstructures and their corresponding diffraction patterns typical of the HAZ at various distances from the weld are shown in Figures 4 through 8. Figure 4 illustrates the microstructure very far from the weld in the base metal (Region I in Fig. 3(b)). The bright field image shows a high density of G.P. zones and the electron diffraction pattern exhibits intense streaks in the <100> directions characteristic of G.P. zones (compare with Fig. 2(a)). Moving closer to the weld (in the direction of increasing peak temperature) a point is reached where reversion of the G.P. zones begins. This is depicted in Figure 5, which shows a much smaller density of zones in the image and less intense streaks in the diffraction pattern as compared with Figure 4. The fully reverted material is shown in Figure 6. Neither the image nor the diffraction pattern shows any evidence of precipitates. The condition closer to the fusion zone is illustrated by Figure 7. Here complete reversion of the G.P. zones has occurred followed by formation of the Θ' precipitate. Reflections due to Θ' are evident in the diffraction pattern and the bright field image shows all three variants of Θ' plates (compare with Fig. 2(c)). The condition of the material closest to the weld is shown in Figure 8. This region is similar to that depicted by Figure 6 and exhibits complete reversion with no subsequent precipitation.

Plate B - Θ"

Figure 9 is a schematic of the metallurgical regions observed after weld-

ing in Plate B, which initially contained only the Θ" precipitate. It can be seen that there are regions of this plate which correspond to similar regions in Plate A. The microstructure of the base metal is shown in Figure 10. The bright field image shows orthogonal sets of plates and the diffraction pattern exhibits the streaks characteristic of Θ" with maxima at 1/4 {200}* 1/2 {200}*, and 3/4 {200}*+. Moving closer to the weld, the first region encountered where metallurgical changes have occurred is one in which the maximum temperature experienced is less than that for the reversion of Θ" to occur. In this region the Θ" array has undergone a transformation from one containing only Θ" to one containing both Θ" and Θ', as shown in Figure 11. The bright field image as well as the diffraction pattern show this to be the case (compare with Figs. 2(b) and 2(c)). Closer to the fusion zone the varying degrees of Θ" reversion are observed. This is shown in Figures 12 and 13. The bright field image in Figure 12 shows a much lower density of Θ" plates than the base metal (see Fig. 10) and the diffraction pattern exhibits only faint streaks. A more advanced stage of reversion is illustrated by Figure 13. This material was located closer to the weld than that depicted in igure 12. Only scattered plates are visible in the image and there are no streaks visible in the diffraction pattern. Figure 14 depicts the condition of the material in a region still closer to the weld. As the bright field image and electron diffraction pattern show, there is no evidence of Θ" but the formation of a few widely scattered plates of Θ' is indicated. Moving toward the fusion zone, the next region encountered has undergone complete reversion of Θ" and re-precipitation of Θ'. The density of Θ' is low near the edges of the region and higher near the center. Figures 15 and 16 illustrate this. Figure 16, which is near the center of the region, shows a high density of Θ' plates. In the region closest to the fusion zone there is complete reversion of Θ" and no re-precipitation of Θ' as the bright field image and diffraction pattern in Figure 17 depict.

Plate C - Θ'

The metallurgical phenomena observed in Plate C after welding are summarized in the schematic Figure 18. It can be noted that the response of this plate, which initially contained the Θ' precipitate, to the welding thermal cycle differs markedly from that of plates initially containing Θ" or G.P. zones (compare with Figs. 3 and 9). Reversion Θ' occurs gradually over a large distance compared to that observed for the smaller precipitates. Figure 19 shows the microstructure of the base metal. The diffraction pattern clearly shows the reflections characteristic of Θ' and the bright field image shows a high density of Θ' precipitates (compare with Fig. 2(c)). The various stages of reversion of Θ' are illustrated by Figures 20, 21, and 22. The microstructure depicted by Figure 20 is at the outside edge of the region of partial reversion. It is apparent from the bright field image that the density of Θ' plates has decreased relative to that in the base metal. Closer to the weld, the density of plates decreases further. This is shown in Figure 21. Moving closer to the fusion zone there is a sparse distribution of plates, as is

+{200}* is the distance between the transmitted spot {000} and the spot due to diffraction from the {200} plane. See Hirsch, et al., Electron Microscopy of Thin Crystals, Krieger Pub. Co., (1977), Chap. 5.

shown in Figure 22. The diffraction pattern, however, shows no evidence of Θ'. It is possible that the precipitates observed are not Θ', but the equilibrium phase, Θ. Closer to the weld, as in plates A and B, there is a region of complete reversion. This is illustrated by Figure 23.

DISCUSSION

The microstructure at any point than as-welded plate is a function of two variables: The microstructure present before welding and the thermal cycle experienced during welding. The pre-weld microstructure is determined by heat treatment and is constant across the width of the plate. The thermal excursion experienced at a point in the heat affected zone or base metal, however, varies as a function of distance from the edge of the fusion zone. Figure 24 shows typical temperature-time profiles that can be expected at different distances from the weld. Curve IV represents the profile at a point very close to the fusion zone. As the distance from the weld increases (denoted by curves III, II, and I), four effects may be noted: (1) the rate of temperature rise decreases, (2) the peak temperature decreases, (3) the maximum cooling rate decreases, and (4) the time to attain the peak temperature increases.

As was shown in the last section, there are different regions observed in an as-welded plate which correspond to particular precipitate transformations. These reactions are somewhat similar in plates A and B, which initially contained G.P. zones and Θ'', respectively. Plate C, which initially contained Θ', produced a markedly different microstructural profile across the cross-section.

The different metallurgical regions of plate A have been depicted in Figure 24 with respect to the temperature-time profiles. The curves I-IV now correspond to the profiles which produced the microstructure observed in those regions of Figure 3(b). Curve I represents the region where the peak temperature achieved was not sufficient to cause any alteration of the initial microstructure (see Fig. 4). The next region closer to the fusion zone is depicted by curve II. The temperature attained was sufficient to cause reversion of the G.P. zones but the time at temperature was insufficient for formation of any other precipitate. The resulting microstructure is a solid solution of copper in aluminum. This was shown in Figure 6. Curve III represents the region in which Θ' formed (see Fig. 7). Here the temperature was in the proper range for a sufficient time for the independent nucleation of Θ' to occur. In the region closest to the weld, the peak temperature achieved was too high for formation of Θ' and the subsequent temperature drop through the regime in which Θ' forms was too rapid for the formation of that precipitate. This microstructure (Fig. 8) is similar to that observed in region II in that complete reversion of the initial G.P. zones occurred with no subsequent precipitation of Θ'. Θ'' was not observed in plate A because the times typical of a welding cycle are not sufficient for its formation (this is supported by the work of Hornbogen[6] on binary Al-Cu alloys).

These same arguments can be applied to the microstructural response of

plate B, with two exceptions. The first is that, at temperatures lower than the reversion temperature ($\sim$ 240°C), a region was observed where the Θ'' structure transformed into one where Θ' had precipitated among the Θ'' plates (see Fig. 11). The formation of Θ' is enhanced greatly by the presence of Θ'' and, as a consequence, the precipitation of the former occurred in a lower temperature regime (farther from the weld) than if Θ had been absent. The second exception is that, in the region of plate B corresponding to region II of plate A, isolated groups of a few plates of Θ' were observed (see Fig. 14). These Θ' plates probably formed among the Θ'' plates in the short time period during the temperature rise through the region which was just discussed and then remained when the Θ'' precipitates reverted upon further increase in temperature.

Plate C, which initially contained Θ', exhibits the simplest metallurgical profile of the three welded plates examined. In the base metal the temperature-time conditions were, by definition, insufficient to induce any alteration of the initial structure. The Θ' precipitates have a much greater diameter and thickness than either Θ'' or G.P. zones and have a body-centered tetragonal structure which results in a semi-coherent interface between the precipitate and the matrix. It is this semi-coherent interface which controls the rate of diffusion under these conditions and, therefore, the reversion process occurs much more slowly than for the smaller, coherent precipitates. This extended region of partial reversion was shown in Figures 20, 21, and 22. The region closest to the fusion zone has the same structure as the corresponding regions in plates A and B. This occurs, regardless of the initial microstructure, because the peak temperature attained is high enough to cause reversion of any precipitate present and the subsequent temperature drop is too rapid to enable precipitation to occur.

CONCLUSIONS

This study examined the effect of the thermal cycle during welding on the microstructure of an age hardening aluminum alloy. Each of three plates of alloy 2219 was heat treated to contain one of the three metastable precipitates of the aluminum-copper binary system (GP zones, Θ'', Θ'). Each plate was subjected to a full penetration autogenous weld pass and the as-welded microstructure was subsequently characterized as a function of distance from the edge of the fusion zone.

It was found that the plates initially heat treated to contain smaller, simpler precipitates (GP zones, Θ'') exhibit four common metallurgical regions: (1) a region of complete reversion, (2) a region of reversion of the initial precipitate and formation of a larger, more complex one (Θ'), (3) a region of complete reversion of the initial precipitate, and (4) the unchanged base metal. In addition, the plate initially containing Θ'' exhibited a region where Θ' had precipitated among the Θ'' plates. The plate which initially contained Θ' exhibited three metallurgical regions after welding: (1) a region of complete reversion, (2) a region of partial reversion, and (3) the base metal. Owing to the size and structure of the Θ' precipitates, the region of partial reversion for this precipitate was much wider than that for the plates initially containing G.P. zones or Θ''.

The results of this study provide direct insight into the structural changes which occur during welding of age hardening alloys. The fact that the observed phenomena occurred within particular temperature-time regimes demonstrates the importance of understanding the kinetics when investigating processes occurring under transient thermal conditions.

ACKNOWLEDGMENTS

This work was supported by The Center for the Joining of Materials under NSF Grant DMR 782-4699.

REFERENCES

1. W. L. Burch, Welding Journal, 37, p 361-5, (Aug. 1958).

2. E. Hornbogen, Aluminum, 43, Pt II, p 9-15 (1967).

3. J. M. Silcock, T. J. Heal, and H. K. Hardy, J. Inst. Metals, 82, p 239 (1953-54).

4. R. H. Beton and E. C. Rollason, J. Inst. Metals, 86, p 77 (1957-58).

5. S. D. Dumolt, D. E. Laughlin, and J. C. Williams, Met. Trans. (submitted).

6. E. Hornbogen, Aluminum, 43, Pt III, p 16-19 (1967).

Table I

Chemical Analysis of 2219 Plate

Element	Al	Cu	Mn	Zr	V	Ti	Fe	Si	Mg	Zn
wt %	bal.	5.7	0.25	0.13	0.11	0.04	0.14	0.06	0.02	0.01

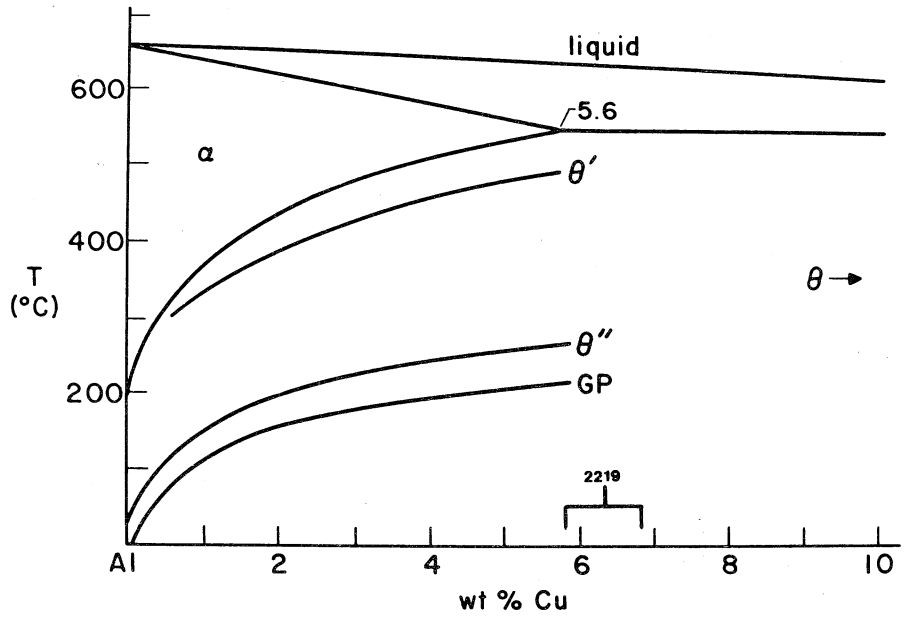

Fig. 1 - Aluminum rich end of the Al-Cu phase diagram. After Hornbogen[2] and Beton and Rollason[4].

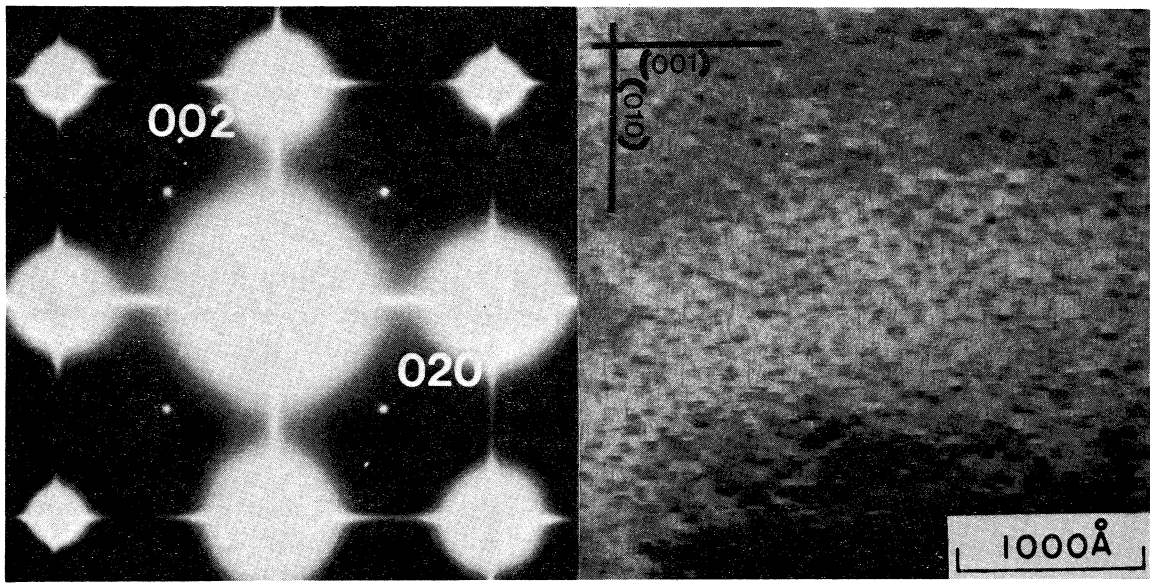

Fig. 2(a) - 100 diffraction pattern and bright field image of alloy 2219 containing GP zones. They exist as monolayers of copper atoms lying on the {100} planes of the matrix and produce streaks in the <100> directions of the diffraction pattern.

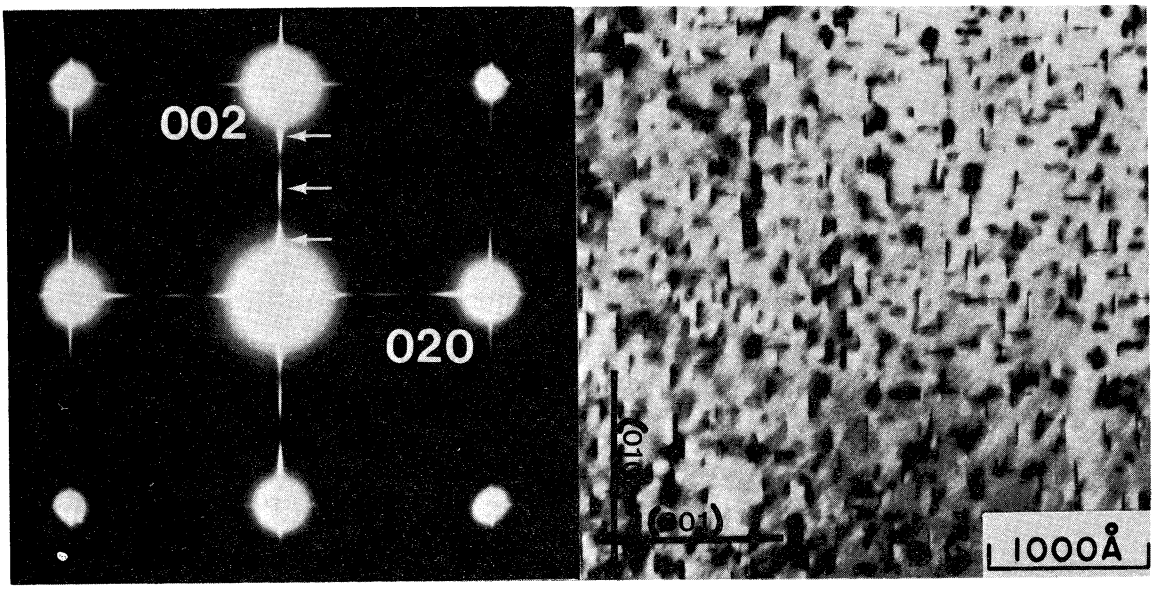

Fig. 2(b) - 100 diffraction pattern and bright field image of alloy 2219 containing Θ" precipitates. They have an ordered structure and exist as plates on the {100} planes of the matrix. The diffraction pattern exhibits streaks with maxima at 1/4 $\{200\}^*$, 1/2 $\{200\}^*$, and 3/4 $\{200\}^*$.

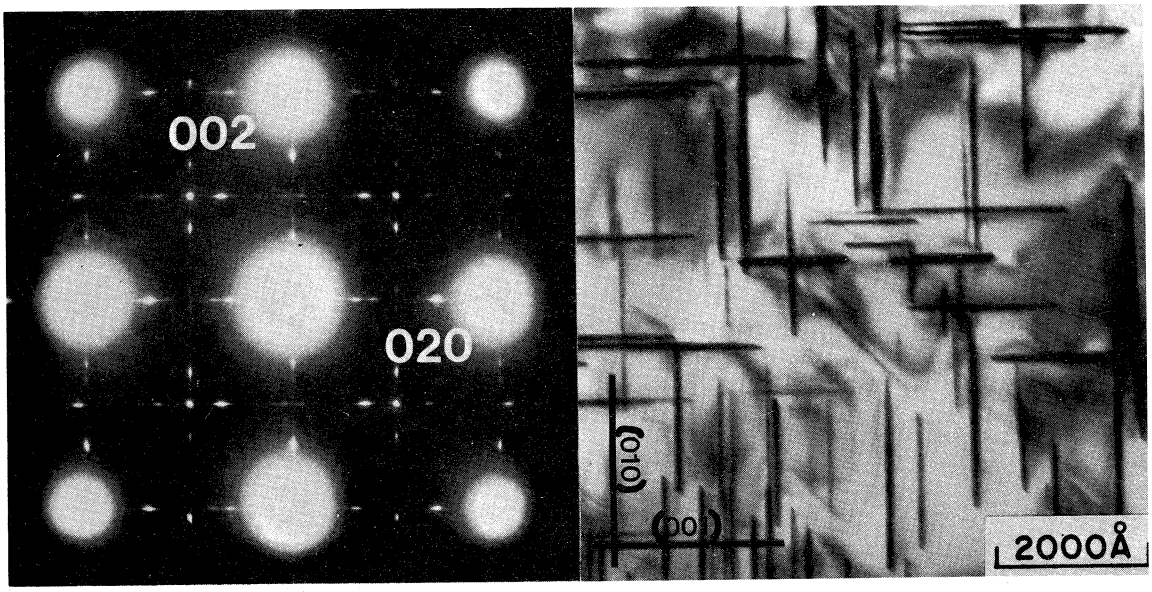

Fig. 2(c) - 100 diffraction pattern and bright field image of alloy 2219 containing Θ' precipitates. They have a body-centered tetragonal structure and exist as plates on the {100} planes of the matrix.

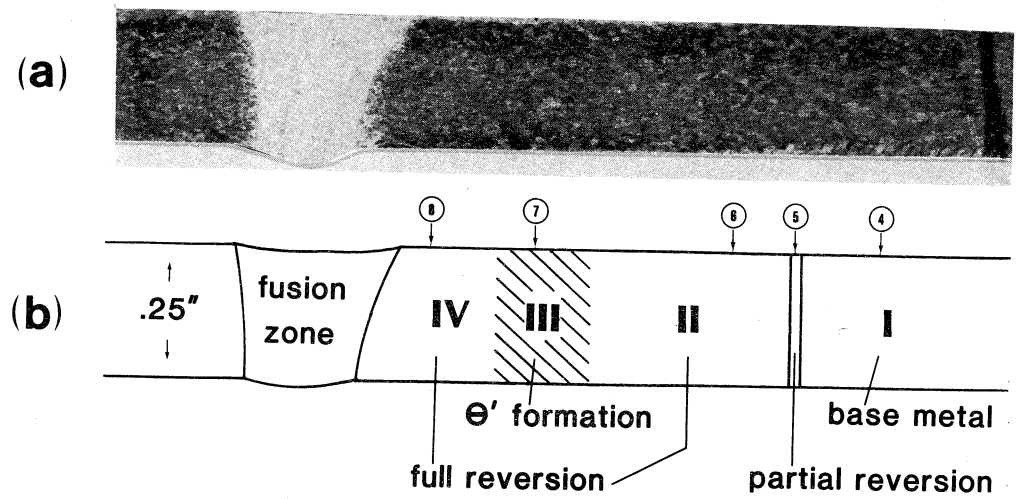

Fig. 3(a) - Cross-section of Plate A after welding. It initially contained GP zones.

Fig. 3(b) - Schematic of Plate A after welding indicating the metallurgical regions observed. Each of the circled numbers in Figures 3, 9, and 18 refers to the figure which illustrates the microstructure observed at that point.

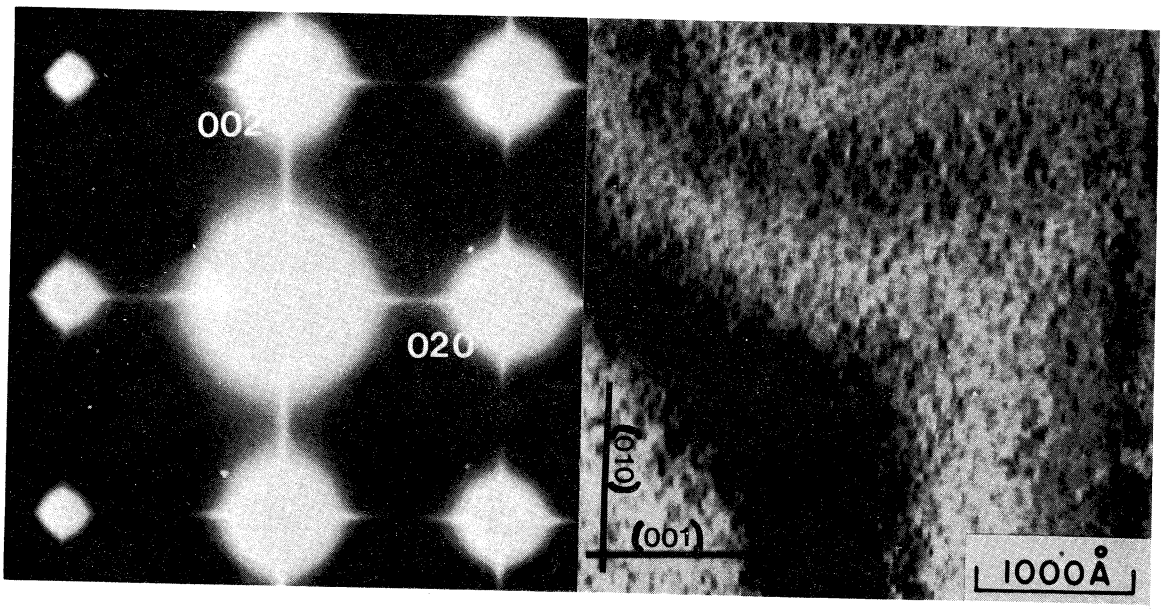

Fig. 4 - Diffraction pattern and image of the microstructure observed in the base metal of Plate A. A high density of GP zones, the original condition of the plate, is represented here.

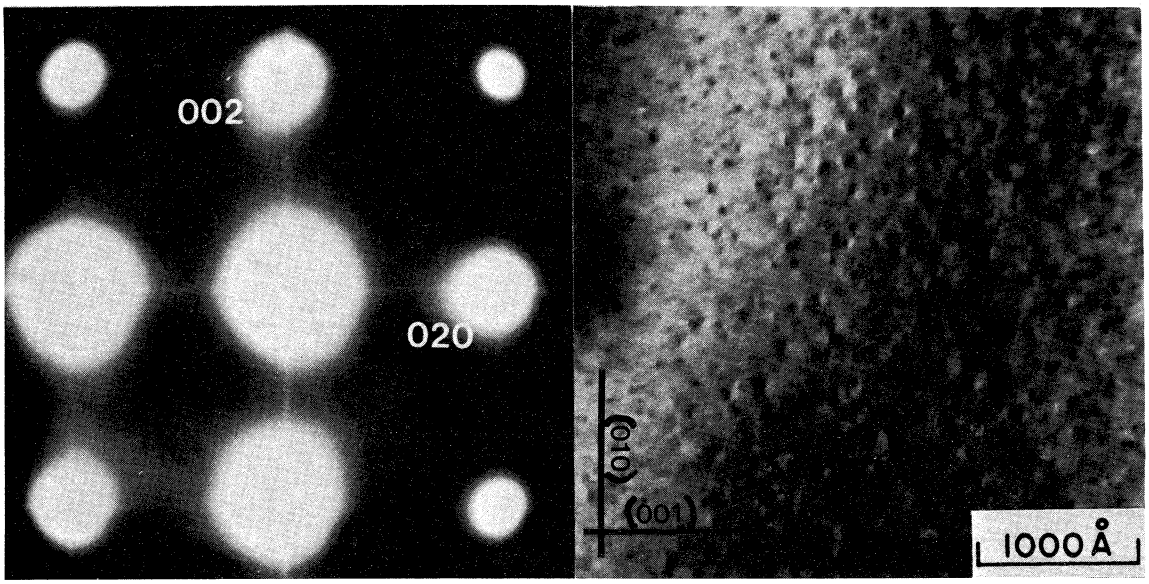

Fig. 5 - Diffraction pattern and image of the microstructure at the edge of the heat affected zone of Plate A, showing partial reversion of the GP zones.

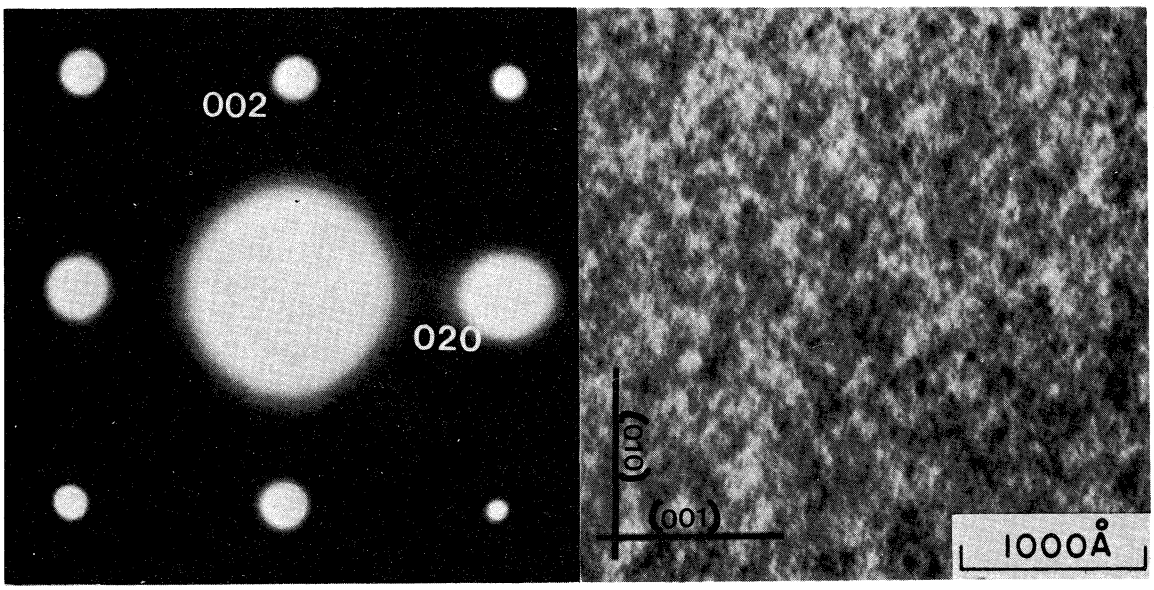

Fig. 6 - Diffraction pattern and image showing complete reversion in region II of Plate A.

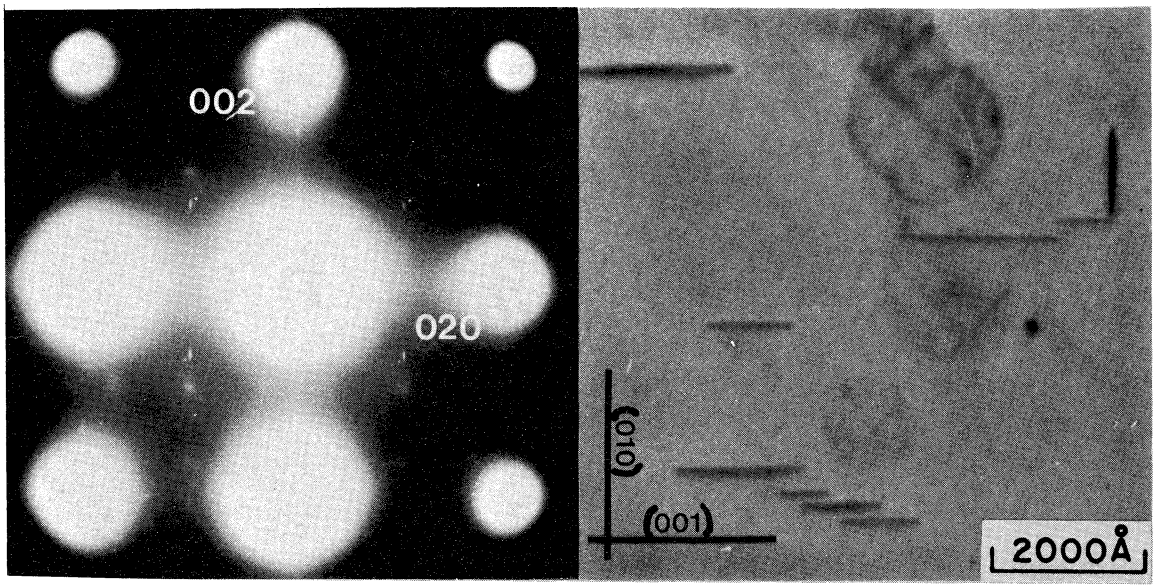

Fig. 7 - Diffraction pattern and image of the region of Plate A where reversion of the GP zones was followed by precipitation of Θ'.

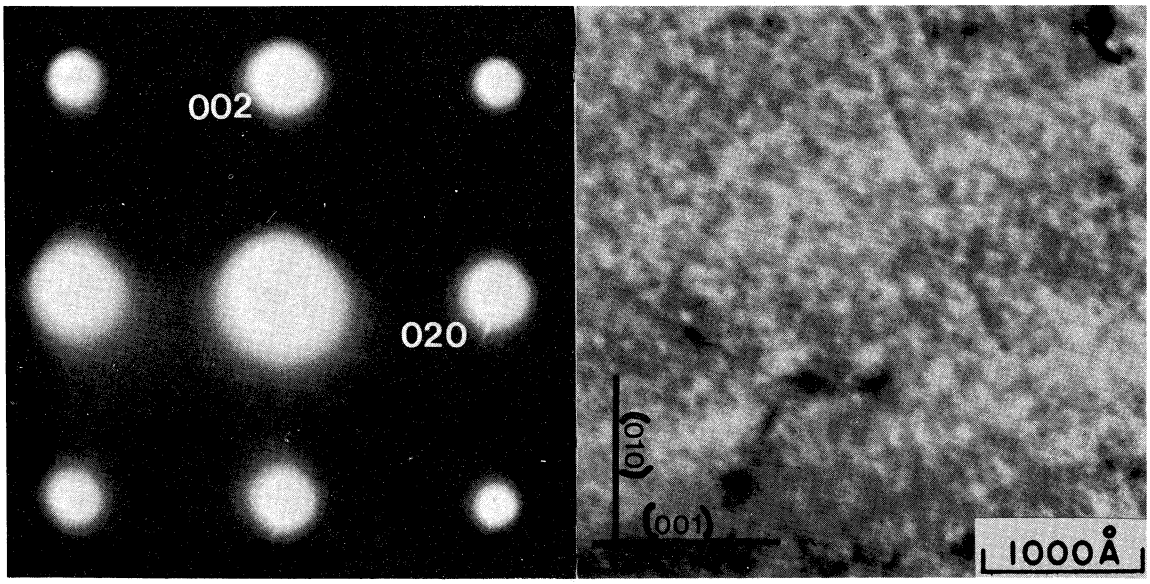

Fig. 8 - Diffraction pattern and image of the microstructure of the region of Plate A closest to the fusion zone. Complete reversion has occurred.

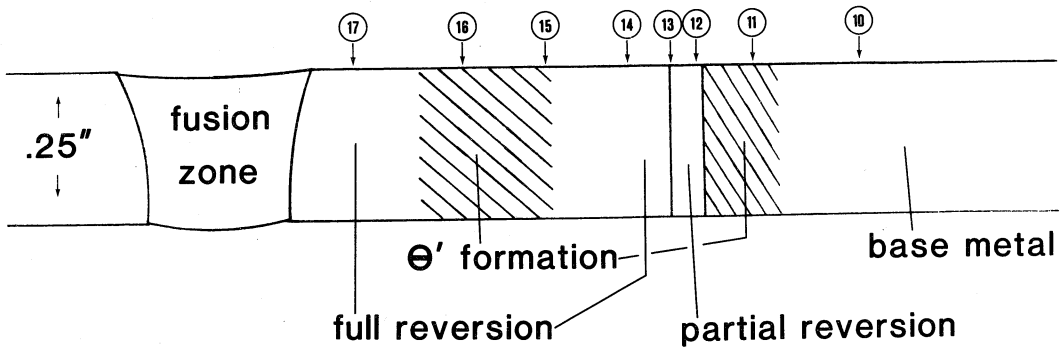

Fig. 9 - Schematic of Plate B after welding indicating the metallurgical regions observed.

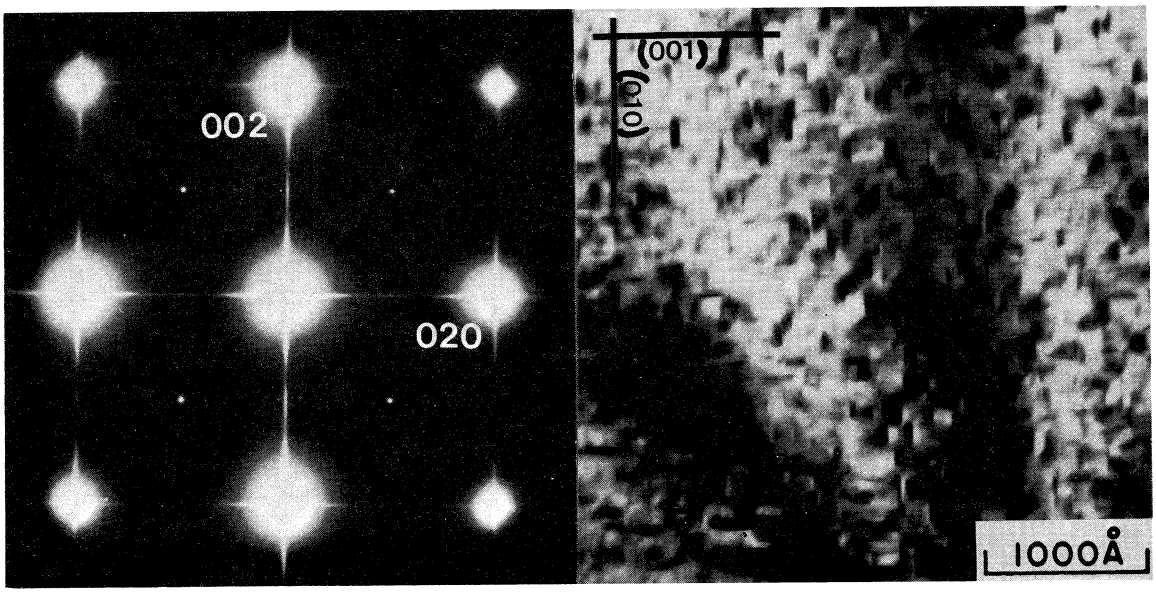

Fig. 10 - Diffraction pattern and image of the base metal in Plate B showing a high density of Θ" precipitates. This was the original microstructure.

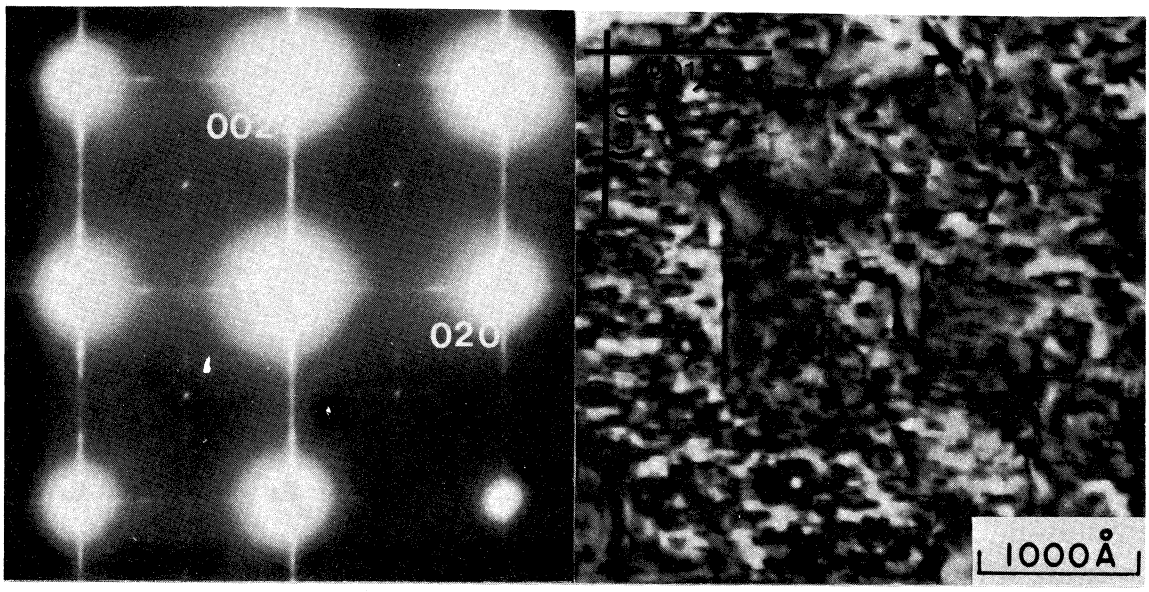

Fig. 11 - Diffraction pattern and image of the region of Plate B where the Θ' phase formed among the plates of Θ".

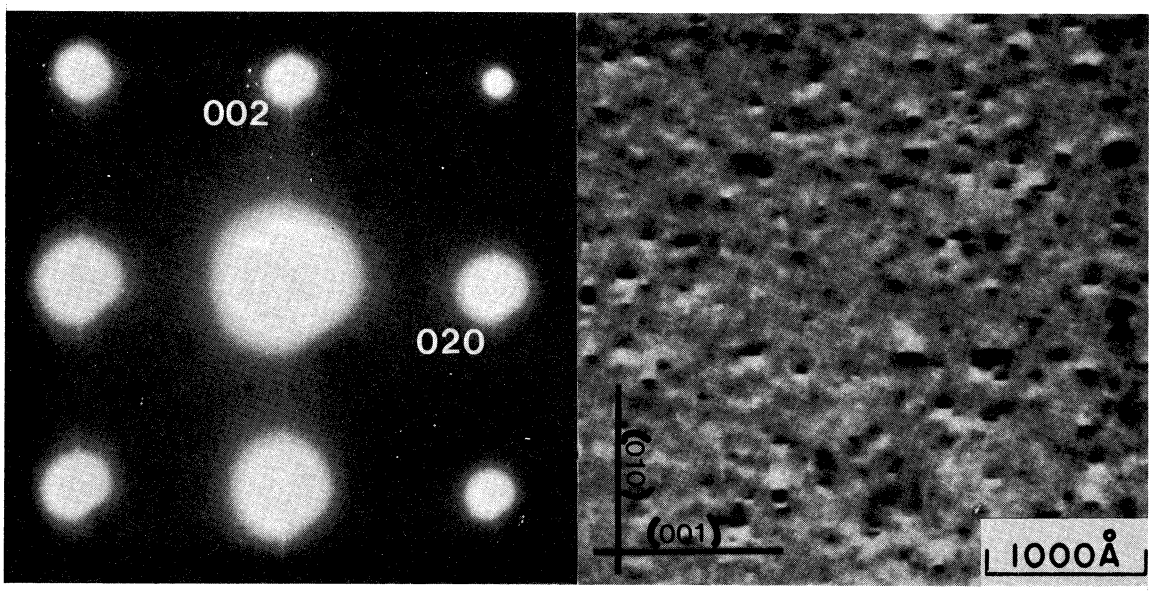

Fig. 12 - Diffraction pattern and image showing partial reversion of Θ" in Plate B.

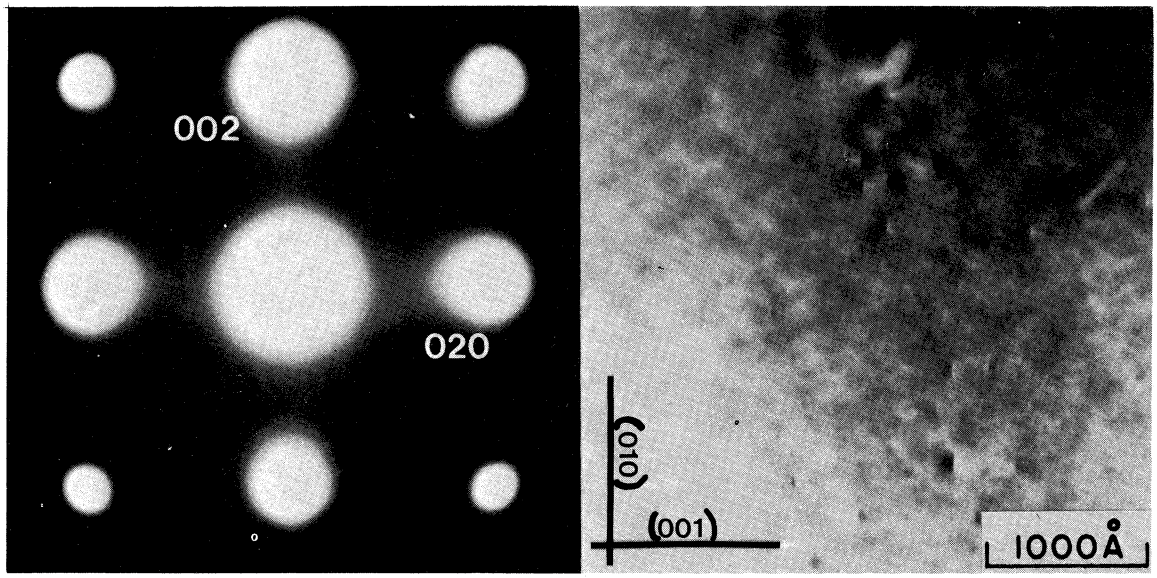

Fig. 13 - Diffraction pattern and image of an advanced stage of Θ" reversion in Plate B. Only scattered plates of Θ" are observable.

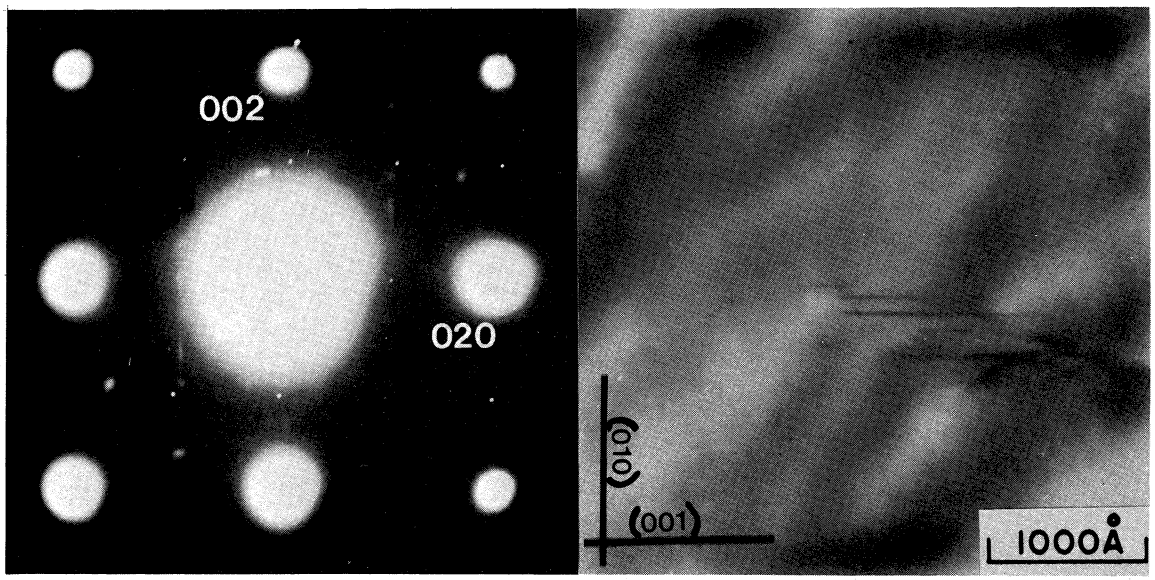

Fig. 14 - Diffraction pattern and image of the region in Plate B where complete reversion of Θ" occurred. Widely scattered groups of Θ' precipitates were observed.

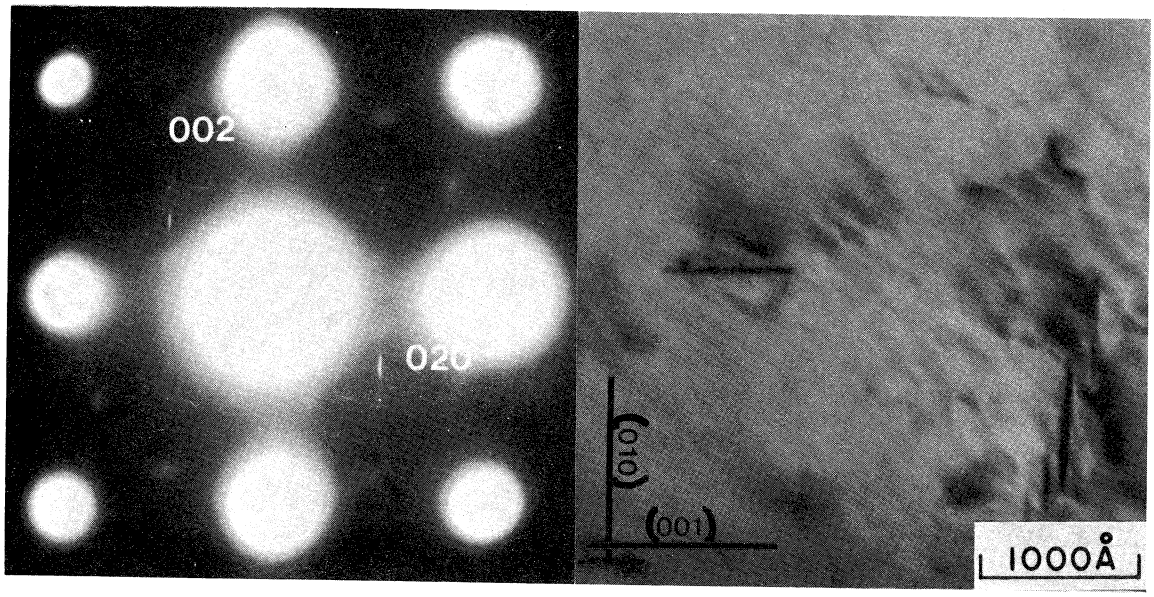

Fig. 15 - Diffraction pattern and image showing the independent formation of Θ' in Plate B. The material depicted here is near the edge of the region and thus has a low density of precipitates (compare with Fig. 16).

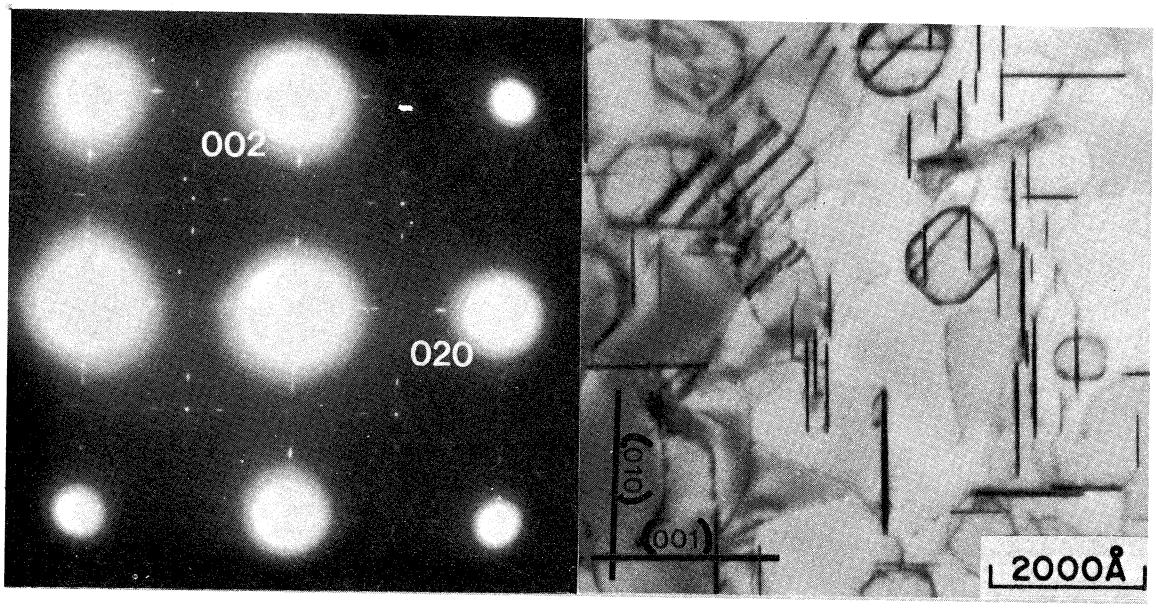

Fig. 16 - Diffraction pattern and image of the region in Plate B where Θ' formed after the reversion of Θ". The material depicted here is located near the center of the region (compare with Fig. 15).

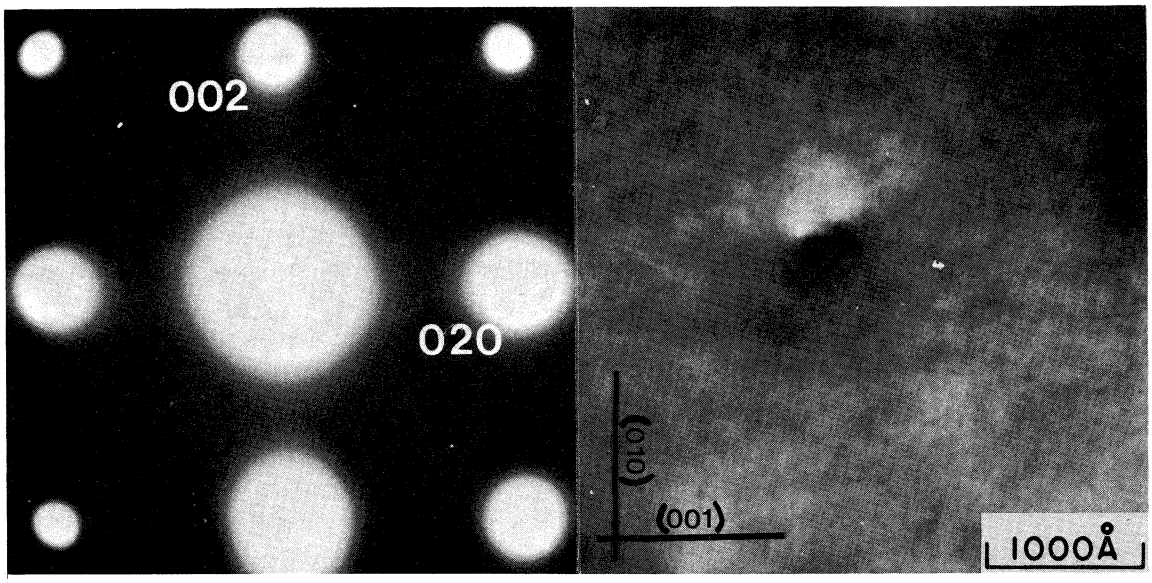

Fig. 17 - Diffraction pattern and image of the region in Plate B closest to the fusion zone. Complete reversion has occurred.

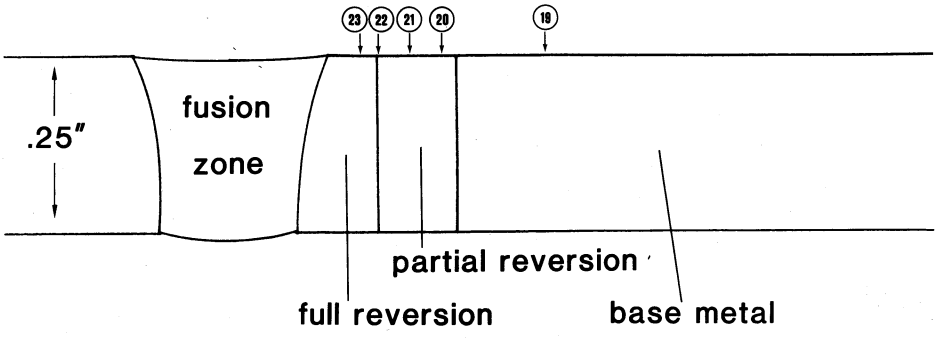

Fig. 18 - Schematic of Plate C after welding indicating the metallurgical regions observed.

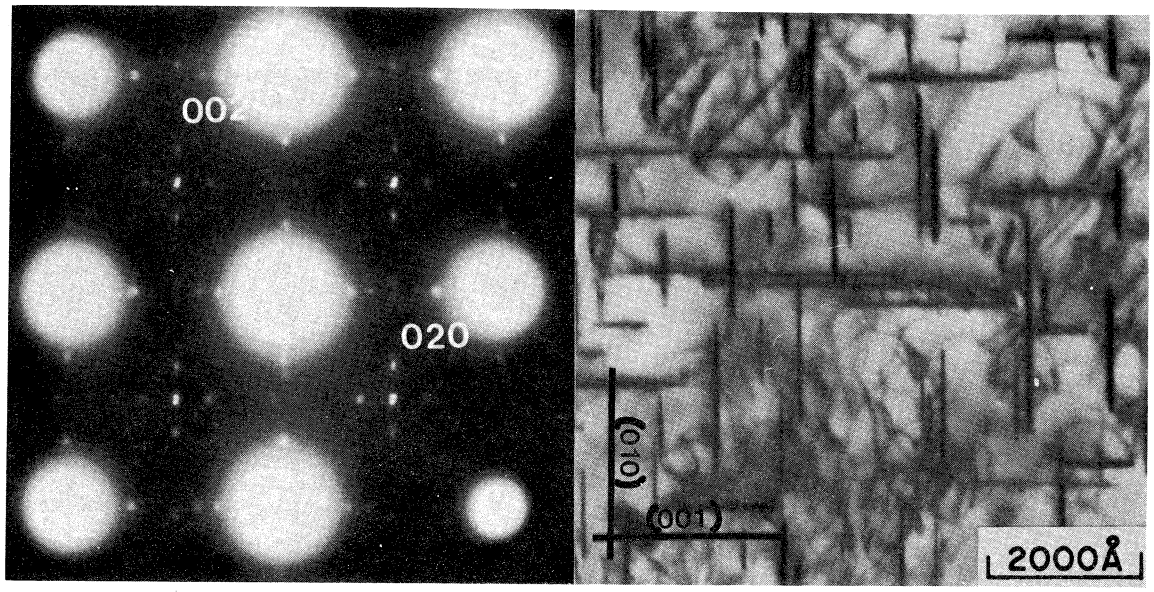

Fig. 19 - Diffraction pattern and image of the base metal in Plate C showing a high density of Θ' plates.

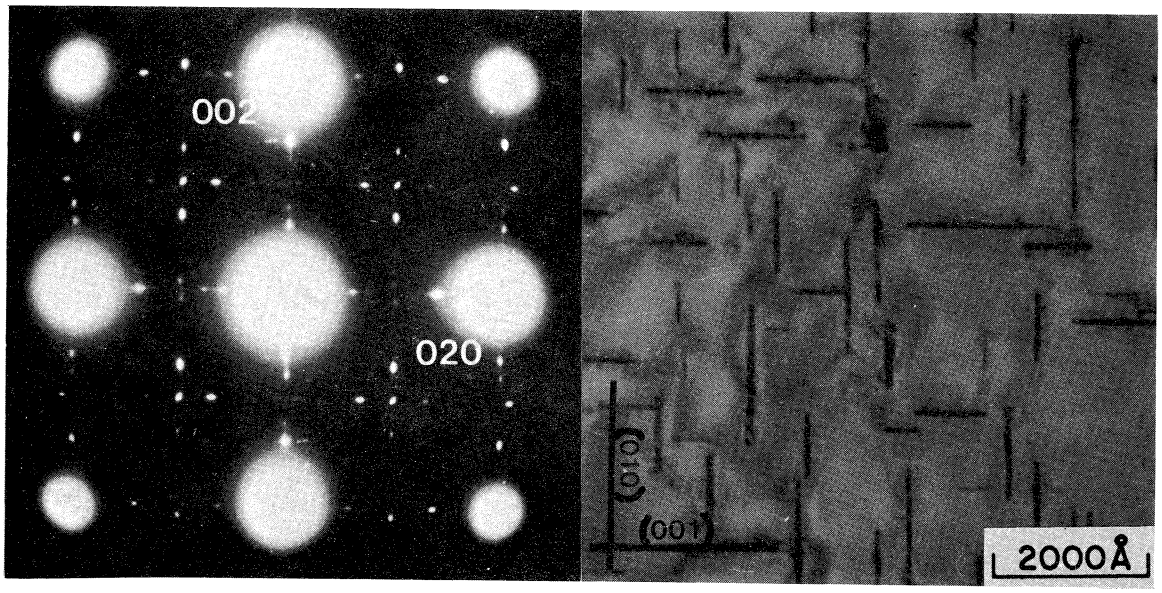

Fig. 20 - Diffraction pattern and image showing the initiation of reversion of Θ' in Plate C. Note the change in precipitate density in Figures 19 through 23.

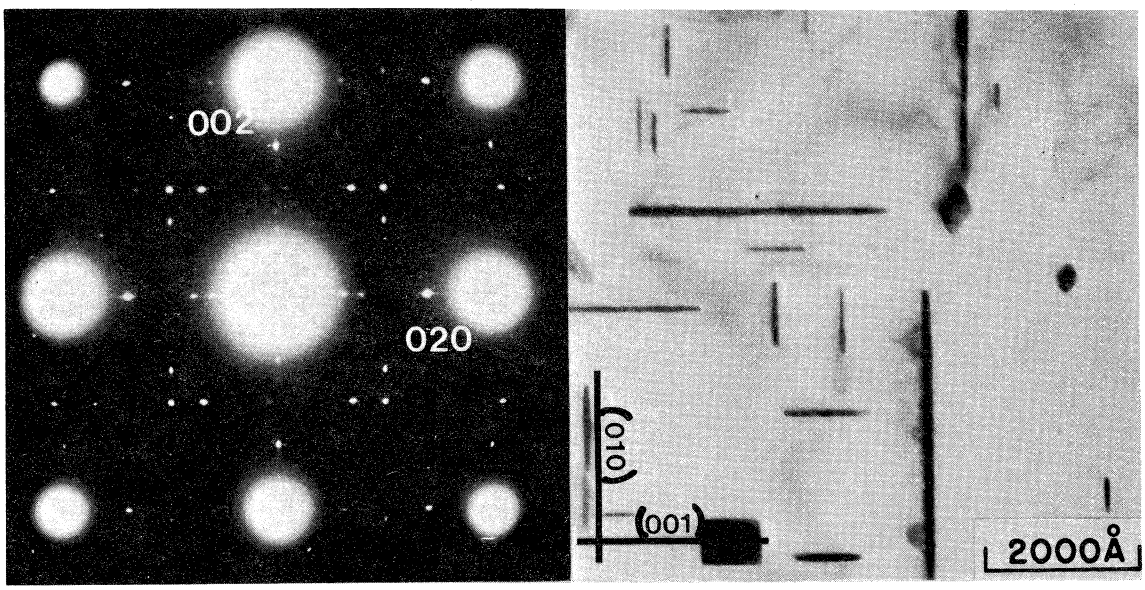

Fig. 21 - Diffraction pattern and image showing an advanced stage of θ' reversion in Plate C.

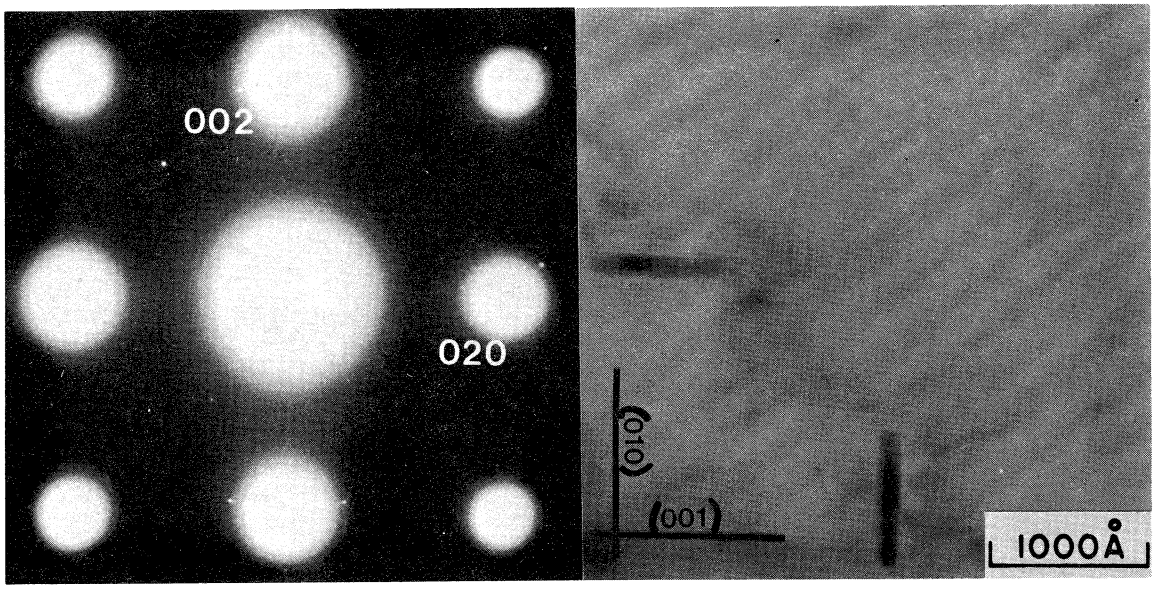

Fig. 22 - Diffraction pattern and image of region in Plate C where reversion is almost complete.

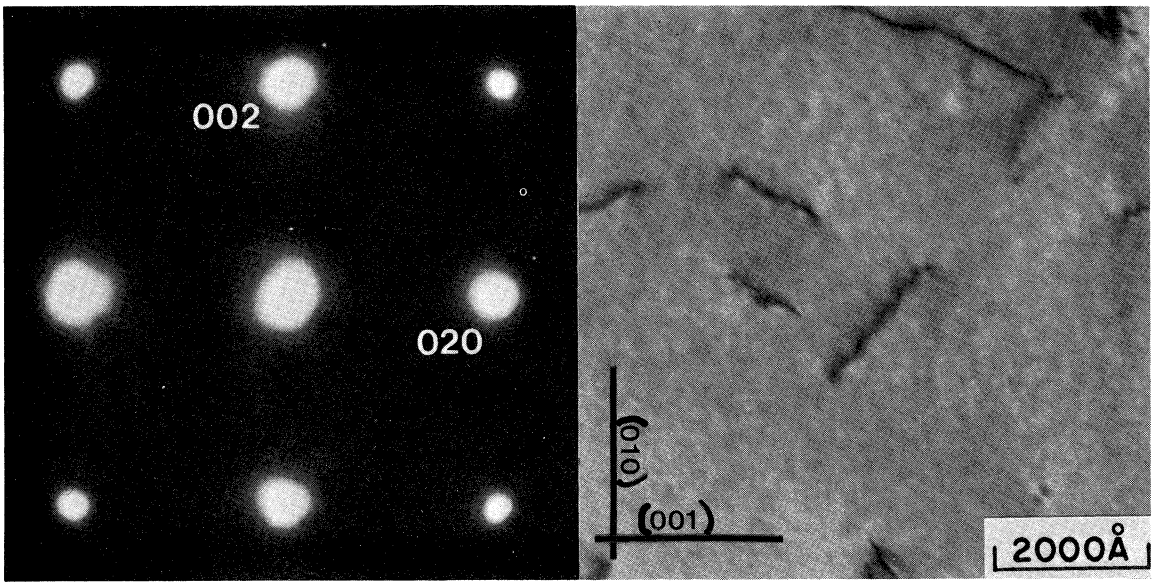

Fig. 23 - Diffraction pattern and image showing complete reversion of Θ' in Plate C.

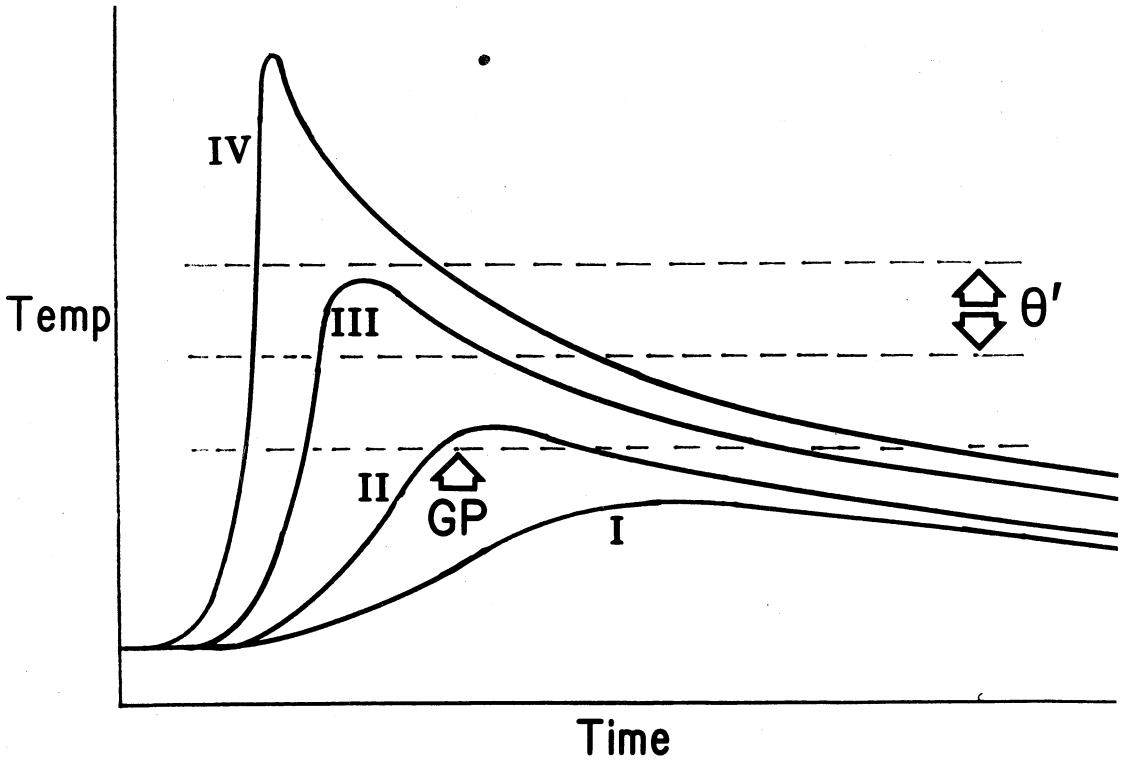

Fig. 24 - Typical temperature-time profiles representing the metallurgical regions observed in Plate A after welding.